Reprinted from SPIE ... 1987 by the Society of Photo-Optical ...

(2)

Laser-generated beam array for commutation of spatially modulated optical signals

J. Taboada

USAF School of Aerospace Medicine, Clinical Sciences Division,
Brooks Air Force Base, Texas 78235-5301

Abstract

A coherent optical method and concept are presented for the generation of an intense, very precisely spaced 2-D array of laser beams which maintain their relative position over significant distances. The array is achieved through the use of a recently invented quadriprism.[1] A signal pattern encoded on a 128x128 array has been precisely transported over several meters. An attractive feature of the system is the low optical energy in the array interstitial space. The interposing of grids or arrays of rectangular lattice electrodes yields very low diffraction losses, thereby making the beam array ideal, e.g., in pipeline processors. Some conceptual applications are discussed.

Introduction

The complex electronic interconnection layout of modern computing devices is becoming more and more the limiting factor in computer development. The massive inherent parallelism of optics thus appears as a very strong alternative for the achievement of vast interconnects. Other advantages of an optical approach for computers will most likely lead to new architectures and software. These additional features include a great ease in input-output coupling, non-interaction of crossing interconnects, and vast holographic memory storage. With improvements in optical bistability devices, even modern optical switching speeds appear to exceed the electronic devices, i.e., of the order of picoseconds (psec).[2] The possible configurations of this new class of computers which use massive optical interconnects will no doubt be numerous and novel. There will likely be in this diversity a common requirement for intense, highly structured beam array patterns to serve as the multidimensional "bus" for communications in the new architectures. In this article, we describe a novel laser method for yielding such a vast uniform array with broadcast and imaged properties simultaneously. The concept is based on a new 2-D generalization of Fresnel's 19th century biprism for interferometric fringe generation. In essence, the quadriprism is introduced for the first time.

The physical optics of the quadriprism interference pattern

The physical optics of the quadriprism are based on the interference of four phase-coherent point sources as described in an earlier article.[3] In the earlier work, a diverging wave front was split by two glass slabs arranged to shear the wave front along orthogonal planes as shown in Figure 1. This arrangement establishes four virtual point sources

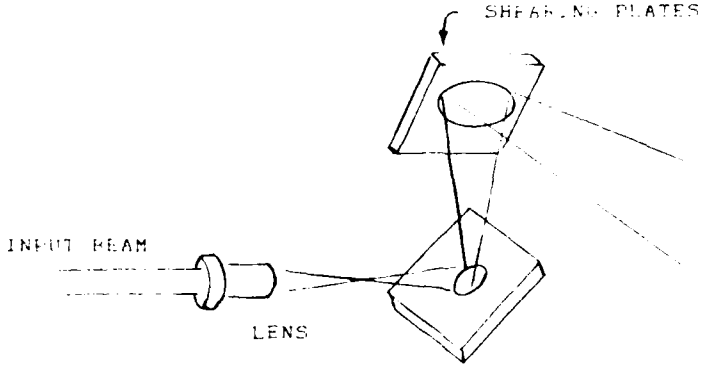

FIG. 1 TANDEM SHEARING PLATES

illustrated in Figure 2. The resulting radiation pattern in the far field can be derived from first principles.

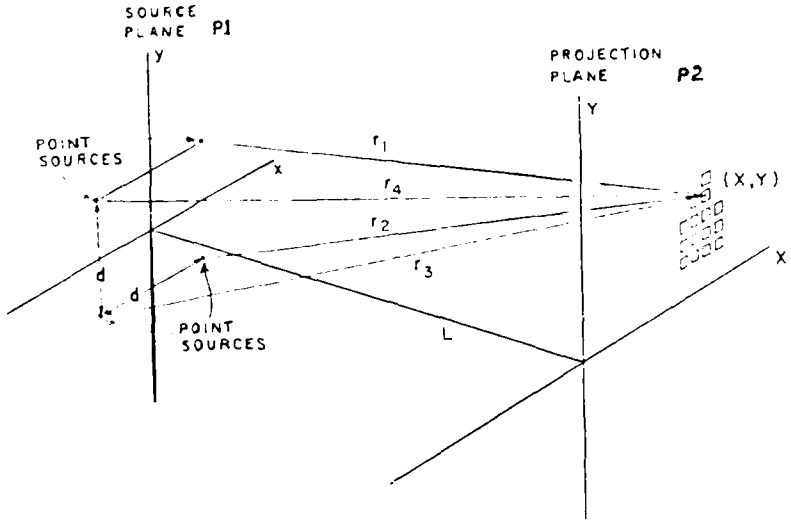

FIG. 2 RADIATION DISTRIBUTION OF 4 COHERENT SOURCES IN THE FAR FIELD

From Figure 2, the point-coherent sources at plane P1 will emanate waves which will propagate to P2, where all four wave fronts will superpose. A scalar superposition of the plane wave fields from each point source is

$$E = E_o e^{-j(\underline{k}\cdot\underline{r}_1 - \omega t)} + E_o e^{-j(\underline{k}\cdot\underline{r}_2 - \omega t)} + E_o e^{-j(\underline{k}\cdot\underline{r}_3 - \omega t)} + E_o e^{-j(\underline{k}\cdot\underline{r}_4 - \omega t)} \quad (1)$$

where $\underline{k}$ is the propagation vector, ω the angular frequency, and E_o is the scalar field amplitude of each source, assumed equal because of the equal reflectivities off the shearing optical flats. The $\underline{r}_1$ to $\underline{r}_4$ are position vectors from each point source. Expanding the position vector terms using the binomial approximation (for example, $r_1 = L + 1/2L[(X-x)^2 + (Y-y)^2]$) and calculating the irradiance term EE^*, we obtain (after extensive algebraic manipulation) for the scalar intensity field at X,Y, due to the

$$EE^* = 16E_o^2 \cos^2\left(\frac{\pi dX}{L\lambda}\right)\cos^2\left(\frac{\pi dY}{L\lambda}\right) \quad (2)$$

interference of the four waves, where E_o is the beam intensity of each point source, d is the separation between the points, L is the distance to the far field point, λ is the wavelength and X and Y are spatial coordinates in the far field. Equation 2 is a rectangular array distribution of square beams with cosine-squared profiles. Also noteworthy is the scaling factor of 16 on the intensity. This latter characteristic indicates the efficiency of light gathering for the far field light pattern.

The novel quadriprism is used to partition a plane (or spherical) wave front into four segments, as shown in Figure 3. The four facets not only create the four coherent sources, but have other useful characteristics. In fact, the pyramid-type prism has, in the knowledge of the author, unique features heretofore escaping application. First, let us consider the action of the single two-facet prism section in one transverse dimension (see Figure 4).

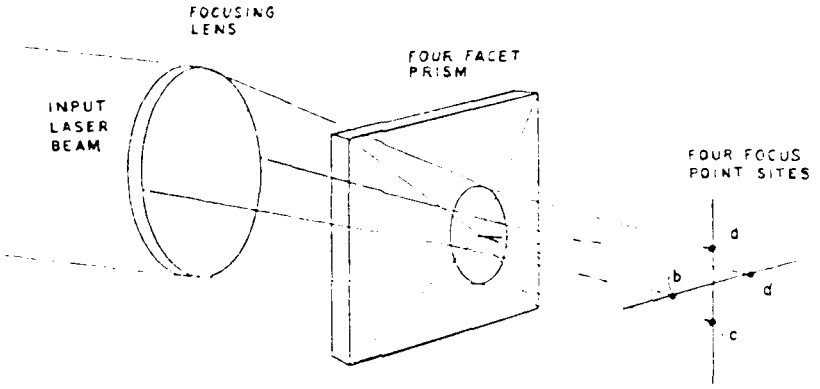

FIG. 3 RAY TRACE CHARACTERISTICS OF THE QUADRIPRISM

Notice that a symmetrically placed beam of diameter (D) as it propagates beyond the prism commences to crossover at the vertex point A, i.e., one half of the beam is folded over the other half. Already with this simple model we see that there will be an optimum plane (B) where the foldover is 100% complete. The location of this plane, which depends on the deviation angle, can be obtained from the geometric ray trace. Note also that there is a very convenient redistribution of the light. The near center of the folded beams, which is more intense for a Gaussian distribution, is relocated to the outside and vice-versa. Essentially, the Gaussian light distribution splits in half, the halves reverse, and then convolve. The result is a dramatically flat distribution of light intensity at (B). The light beyond this plane separates to form individual beams at (C). The beams will exhibit interference phenomena where they intersect and generate fringe lines. The number of fringe lines at the plane (B) can be derived as follows.

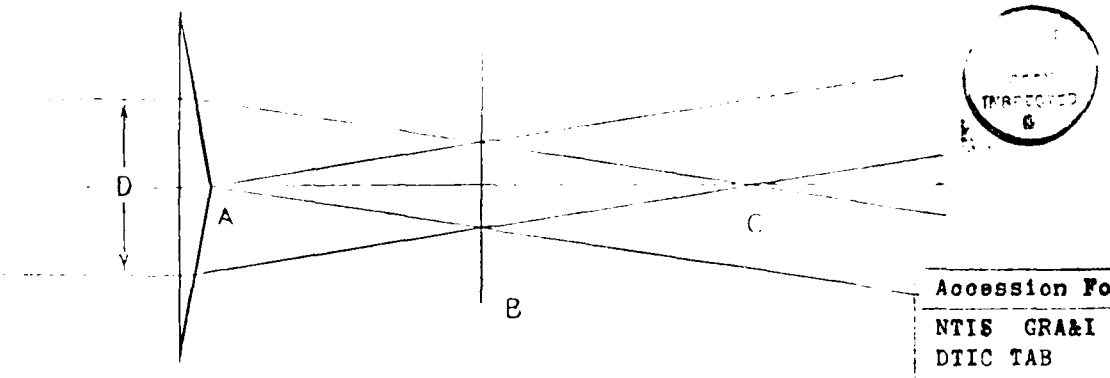

FIG. 4 EFFECT OF TWO QUADRIPRISM FACETS ON COLLIMATED LASER INPUT BEAM

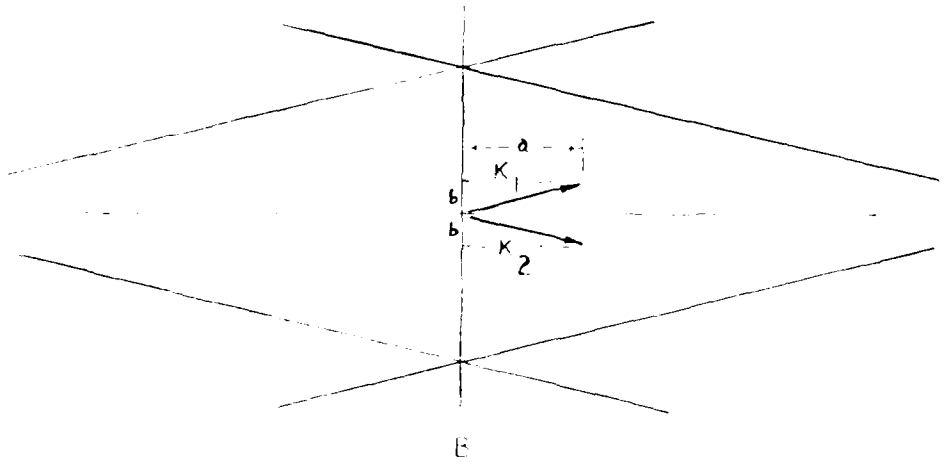

FIG. 5 WAVEFRONT VECTORS IN THE OVERLAP REGION

Consider a more detailed diagram of the intercept region as shown in Figure 5. At the origin of plane (B), the incident plane waves project respective wave vectors $\underline{K}_1$ and $\underline{K}_2$. These wave vectors have x and y projections (a,b) and (a,-b) respectively; that is

$$\underline{K}_1 = \frac{2\pi}{\lambda}(a\hat{i} + b\hat{j})/\sqrt{a^2 + b^2},$$
$$\underline{K}_2 = \frac{2\pi}{\lambda}(a\hat{i} - b\hat{j})/\sqrt{a^2 + b^2}, \tag{3}$$

where the $\hat{i}$ and $\hat{j}$ are unit vectors, the radical expresses the appropriate normalization of the vector, and λ is the wavelength. We next ask, what is the resultant field intensity at $y\hat{j}$ along the (B) plane? We resort to the linear superposition of electromagnetic fields expressed as the quantity

$$E(r) = Ae^{j(\underline{K}_1\cdot\underline{r} - \omega t)} + Ae^{j(\underline{K}_2\cdot\underline{r} - \omega t)}, \tag{4}$$

where A is a scalar amplitude of the two waves, here assumed equal for the two partial waves; $\underline{r} = y\hat{j}$, ω = angular frequency of the wave. The intensity of the resultant light distribution at $(\underline{r})$ is given by the real quantity

$$\begin{aligned} I &= \mathrm{Re}[E(\underline{r})E^*(\underline{r})] \\ &= \mathrm{Re}\{[Ae^{j(\underline{K}_1\cdot\underline{r})} + Ae^{j(\underline{K}_2\cdot\underline{r})}][A^*e^{-j(\underline{K}_1\cdot\underline{r})} + A^*e^{-j(\underline{K}_2\cdot\underline{r})}]\} \\ &= \mathrm{Re}\{AA^* + A^*A + AA^*e^{j(\underline{K}_1 - \underline{K}_2)\cdot\underline{r}} + A^*Ae^{j(\underline{K}_2 - \underline{K}_1)\cdot\underline{r}}\} \\ &= 2AA^* + AA^*[\cos[(\underline{K}_1 - \underline{K}_2)\cdot\underline{r}] + \cos[(\underline{K}_2 - \underline{K}_1)\cdot\underline{r}]] \end{aligned} \tag{5}$$

The cosine function is symmetric, thus

$$I = 2AA^*[1 + \cos(\underline{K}_1 - \underline{K}_2)\cdot\underline{r}]. \tag{6}$$

Substituting for $\underline{K}_1$, $\underline{K}_2$, and $\underline{r}$, that is

$$(\underline{K}_1 - \underline{K}_2)\cdot\underline{r} = \frac{2\pi}{\lambda}\left(\frac{[a\hat{i} + b\hat{j}]}{\sqrt{a^2 + b^2}} - \frac{[a\hat{i} - b\hat{j}]}{\sqrt{a^2 + b^2}}\right)\cdot y\hat{j}$$
$$= \frac{2\pi}{\lambda}\frac{2by}{\sqrt{a^2 + b^2}} \tag{7}$$

Therefore,

$$I(y) = 2AA^*\left(1 + \cos 2\left(\frac{2\pi}{\lambda} \cdot \frac{by}{\sqrt{(a^2 + b^2)}}\right)\right). \tag{8}$$

Or, by a trigometric identity,

$$I(y) = 4AA^*\cos^2\left(\frac{2\pi}{\lambda} \cdot \frac{by}{\sqrt{(a^2 + b^2)}}\right). \tag{9}$$

Indeed, we note that the light intensity is exactly periodic along y with spatial period spacing $\lambda\sqrt{(a^2+b^2)}/b$. A similar analysis is obtained for the perpendicular axis. The quantity $b/\sqrt{(a^2+b^2)} = \sin\theta$, where θ is the angle the wave front makes with the optical axis. Also, θ is one-half the total deviation angle δ of the biprism. The fringe spacing Δy is therefore given by the quantity

$$\Delta y = \frac{\lambda\sqrt{(a^2 + b^2)}}{b} = \frac{\lambda}{\sin\theta} = \frac{\lambda}{\sin(\delta/2)}. \tag{10}$$

The number of fringes (N) is thus given by

$$N = \frac{D\sin(\delta/2)}{2\lambda}. \tag{11}$$

It was unexpected, but discovered to be the case, that the pattern, once generated, could be recollimated and transmitted with the periodic transverse distribution through large ranges of space. For various applications at hand, the optical system was designed to give a value of N of about 128. This can be accomplished through a number of variables, noting from equation 11, D, λ and δ, all of which can be varied. The quantity δ depends on the index of the media surrounding the vertex of the prism.

Experimental prototype system

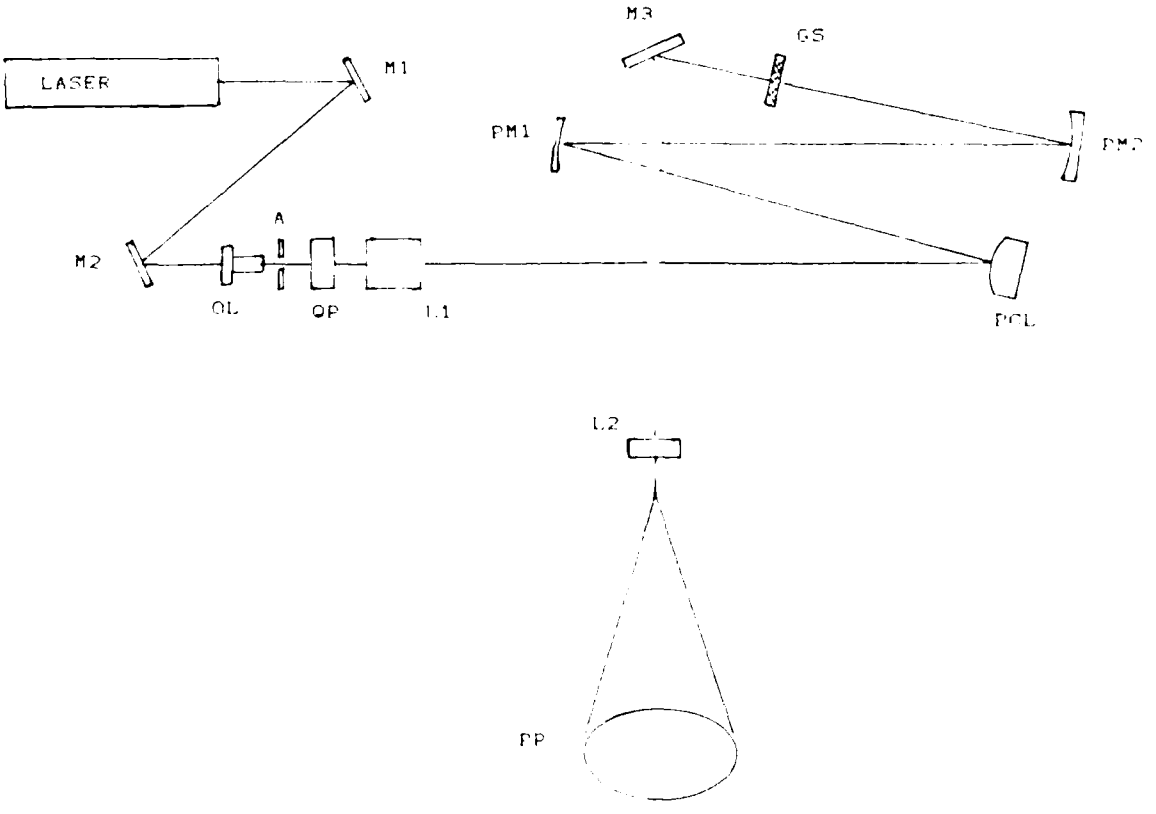

FIG. 6 LABORATORY PROTOTYPE OPTICAL SYSTEM

An experimental prototype arrangement for the generation of the array pattern is shown in Figure 6. Here, a 100 mW Ar-ion laser beam (514 nm wavelength) is spatially filtered by a 10x microscope objective lens (OL) and 25 micron pinhole aperture (A). The quadriprism (QP), a four-facet, 50 mm diameter component manufactured by Precision Optical and having arc second precision, 1° - elevation facets, is inserted in the expanding optical region. As expressed by equation 11, this allows linear control of the number of array elements through the diameter (d) variable. In the absence of the quadriprism, the collimating lens (L1), f=250 mm, d=56 mm, collimates an otherwise Gaussian beam to a diameter of about 25 mm.

The action of the quadriprism is such that the Gaussian beam is folded over at a range of 100 cm; the radiation pattern is remarkably square, distributed as shown in Figure 7. Within the square, about 15 mm, the light distribution contains about 80% of the beam power and is highly structured, as given by equation 2. The camera does not resolve the array, but it is clearly observed by tilting a target screen.

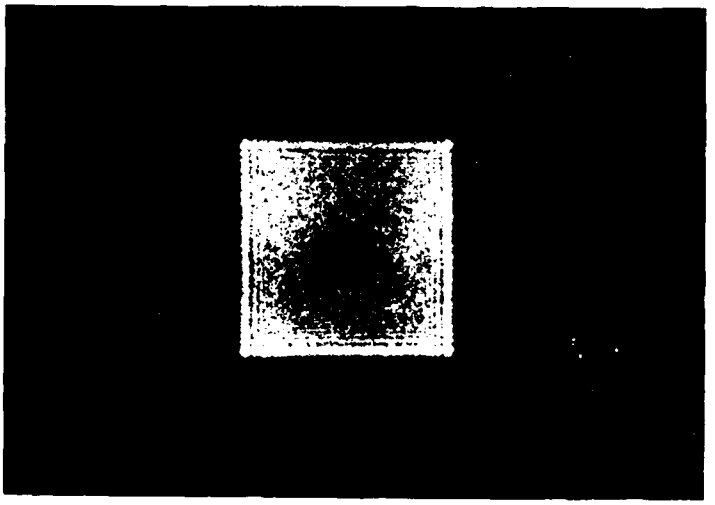

FIG. 7 PHOTOGRAPH OF LIGHT DISTRIBUTION AT INPUT TO SECOND EXPANSION TELESCOPE

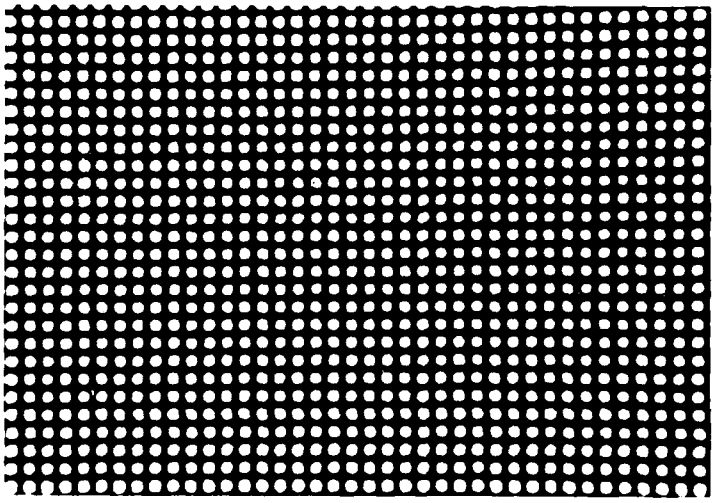

FIG. 8 PHOTOGRAPH OF BEAM ARRAY IN LIGHT IN PLANE II

The array pattern can be expanded or contracted. In the optical arrangement of Figure 6, the pattern was expanded and recollimated into a 64 mm square containing 128x128 elements. The expansion and recollimation was accomplished with a telescope consisting of a photo copier lens (PCL), MFax Topcor 4.5/130, and parabolic mirrors PM1 and PM2, 102 mm by f=228 mm and 190 mm by f=503 mm.

The collimated pattern is propagated for 0.5 m and passed through a 128x128 grid screen (GS) to test the sensitivity to alignments. The pattern size and orientation can be easily adjusted by appropriate precision motion of the quadriprism in X-Y and axial rotation. The matching condition was easily detected by observing the Moiré pattern caused by any slight error in spatial period. The pattern was further propagated without noticeable changes over a distance of 0.7 m without noticeable changes to a positive lens L2, f=120 mm. In the focal plane of this lens, one can observe the four virtual point sources within about a 1.5 mm square. The pattern after this point, of course, diverges such that, at a range of 1.24 m, the pattern covers a spot 0.8 m in diameter at the projection plane (PP). A photograph of this pattern is shown in Figure 8.

The optical system exhibited other characteristics of importance for potential optical computing applications. For example, a very small dove prism, 5 mm aperture, could be placed at the focal point of L2 to achieve matrix-like transposition of the elements. Also, any subset could readily be diverted out of the path by a prism. An application of the highly structured light is evident for robotic vision devices for the automation of surface metrology. An example of a pattern projected on familiar objects is shown in Figure 9 and on a wrinkled piece of paper in Figure 10. The pattern will be encoded with a

FIG. 9 PHOTOGRAPH OF BEAM ARRAY INCIDENT ON FAMILIAR OBJECTS

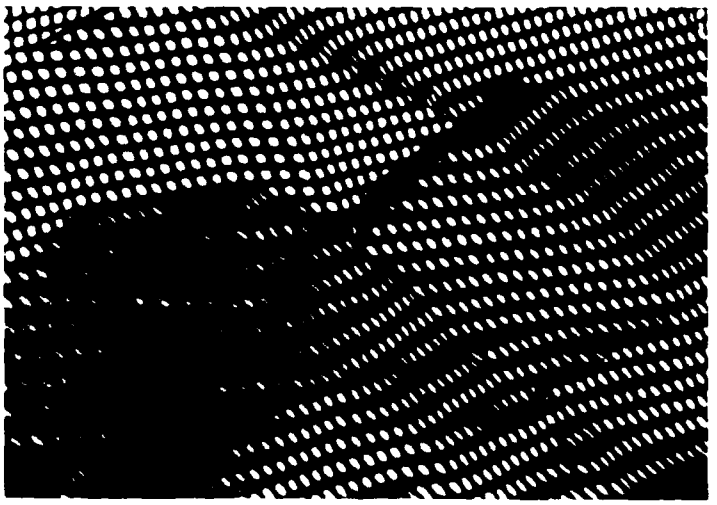

FIG. 10 PHOTOGRAPH OF BEAM ARRAY INCIDENT ON A WRINKLED SHEET OF PAPER

spatial light modulator such as a Hughes Aircraft model H4060. The structured beam array pattern, emanating from a virtual point coupled with encoding and computer-controlled camera image acquisition, will yield high-speed surface maps; however, the optical computer applications of the system also may be quite far-reaching.

Optical computer applications

Many different architectures are being proposed for optical computers.[4,5] A common approach is the optical pipeline processor. For example, A. Huang has demonstrated that optical digital computing can be obtained by pipeline arrangements of "functional logic blocks" which can manipulate on optical bistable gates the 16 Boolean connecting functions of two variables.[6] Ichioka and Tanida propose a shadow mask arrangement to affect the functional blocks.[7] In Ichioka's and Tanida's proposal, the masks, which are the pipeline processing elements, are restricted to very short-range distances by a scalar diffraction

$$4\lambda < l << b^2/\lambda \tag{12}$$

expression (equation 12) where λ is the wavelength of the illumination, l is the mask separation, and b is the aperture size. For a dense array 256x256 on reasonable laboratory scales, b=0.3 mm would imply a restricted value for l, l<<10 cm. The optical system discussed above can resolve this restriction, extending the mask-to-mask region to several meters. Thus a very dense pipeline processor can be achieved.

A concept for a pipeline optical processor is schematically illustrated in Figure 11. The inputs in the form of optical beam arrays are simultaneously commuted to a CPU controller and to a pipeline array. The system is activated by several array working signals. The CPU controller accesses in parallel a memory section as well as the pipeline array.

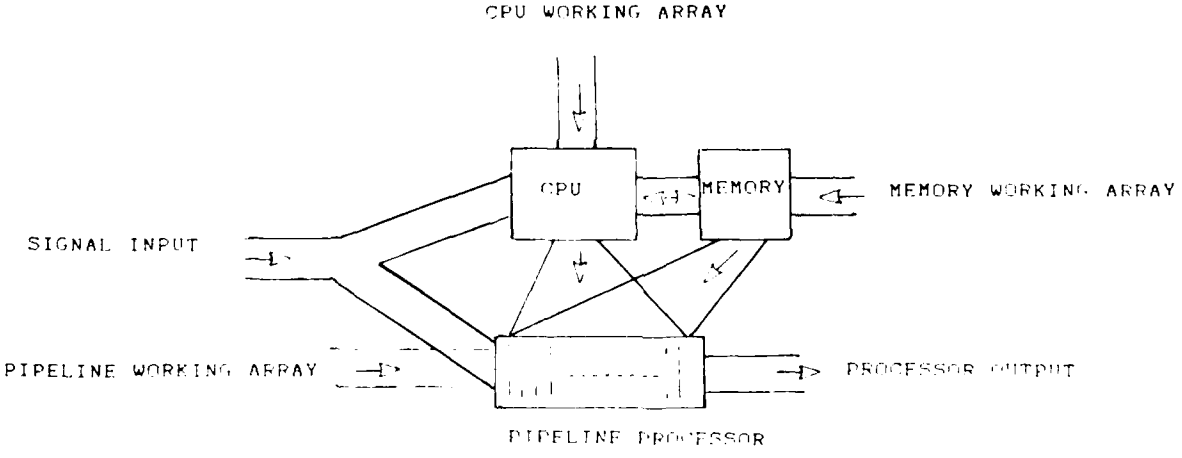

FIG. 11 PROPOSED OPTICAL PIPELINE PROCESSOR COMPUTER

This system would have massive computational capability. For example, consider 1,000 gateable masks controlled along the pipeline having 256x256 arrays within a 3 m region of space. Then, assuming switching could be accomplished in 100 psec, such a system would have a computational yield of

$$\text{operational bits/second} = \frac{(256) \times (256) \times 1000}{\frac{3\text{m}}{3 \times 10^{8}\ \text{msec}^{-1}} + 1000 \times (100 \times 10^{-12}\ \text{sec})} = 6.0 \times 10^{14} \tag{13}$$

This amazing computational yield would, of course, far exceed even the fastest computer systems available at present; however, there remain significant communication problems to resolve before such a processor can be realized.

Acknowledgements

Helpful technical support by Mr. Heinz Jaeger of the Instrumentation Shop and SSgt Mario Villanea is acknowledged.

References

1. U. S. patent 4,523,809 "Method for and apparatus for generating a structured light beam array." Inventors: J. Taboada and B. R. Altschuler, June 18, 1985.

2. Smith, P. W. and Tomlinson, W. J., "Bistable optical devices promise subpicosecond switching," IEEE Spectrum, vol. 18, no. 6, pp. 26-33. 1981.

3. Taboada, J., "Coherent optical methods for applications in robot visual sensing," Society of Photo-optic Instrumentation Engineers, vol. 283, pp. 25-29. 1981.

4. Sawchuk, A. A., "Digital optical computing," Proceedings of the IEEE, vol. 72, no. 7, pp. 758-779. 1984.

5. Yatagai, T., "Cellular logic architectures for optical computers," Applied Optics, vol. 25, no. 10, pp. 1571-1577. 1986.

6. Huang, A., "Architectural consideration involved in the design of an optical digital computer," Proceedings of the IEEE, vol. 72, no. 7, pp. 780-786. 1984.

7. Ichioka, Y., and Tanida, J., "Optical parallel logic gates using a shadow-casting system for optical digital computing," Proceedings of the IEEE, vol. 72, no. 7, pp. 787-801. 1984.